

Enhanced dielectric and piezoelectric properties of $x\text{BaZrO}_3-(1-x)\text{BaTiO}_3$ ceramics

Liang Dong,^{1,2} Donald S. Stone,² and Roderic S. Lakes^{1,2,3,a)}

¹Department of Engineering Physics, University of Wisconsin, Madison, Wisconsin 53706-1687, USA

²Materials Science Program, University of Wisconsin, Madison, Wisconsin 53706-1687, USA

³Engineering Mechanics Program, University of Wisconsin, Madison, Wisconsin 53706-1687, USA

(Received 4 September 2011; accepted 24 March 2012; published online 24 April 2012)

$x\text{BaZrO}_3-(1-x)\text{BaTiO}_3$ solid solutions ($x = 0, 0.04, 0.06, 0.08, 0.12,$ and 0.18) synthesized via conventional solid state reaction method exhibit piezoelectric coefficients comparable to those of “hard” PZT-8, PZT-4, and even “soft” PZT-5 A. Doping also improves the poling efficiency of $x\text{BaZrO}_3-(1-x)\text{BaTiO}_3$ ceramics. Study of temperature dependence of the dielectric and piezoelectric properties reveal the following. Doping lowered the Curie point but raised the temperatures of the other two transformations. The diffused phase transition behavior has been enhanced with increasing content of BaZrO_3 , but $x \leq 0.18$ is not enough to show a relaxor behavior. Piezoelectric responses show peaks at transformation temperatures and exhibit the best stability in the orthorhombic phase. Significant improvement in room temperature piezoelectric and electromechanical responses ($d_{33} = 420\text{pC/N}$, $d_{31} = -138\text{pC/N}$, and $k_p = 49\%$) comparable to PZT-5 A is achieved at a composition of $x=0.06$ (1400 °C 100 h sintered), which brings the rhombohedral-orthorhombic transition to the ambient temperature. Enhanced piezoelectric properties are mainly attributed to a series of microscopic phase transformations due to the presence of internal structural gradient. Other possible contributions such as domain structures and constrained negative stiffness effect have also been discussed. © 2012 American Institute of Physics. [<http://dx.doi.org/10.1063/1.4705467>]

I. INTRODUCTION

Piezoelectric materials convert electrical signals to mechanical deformation or the reverse. They are used widely in sensors and actuators, such as microphones, acoustic emitters, ultrasonic sensors and emitters, and actuators. Lead oxide based ferroelectrics, such as lead titanate zirconate, are widely used for such applications due to their excellent piezoelectric properties.¹ They offer good sensitivity but contain lead which is dense and toxic; Lead is also reactive so that processing of such materials is challenging. Lead free materials, therefore, offer potential benefits. The search for better materials is driven in part by the expansion of applications of such materials. It is often possible to enhance piezoelectric sensitivity by varying the composition to lower the Curie temperature² to obtain “soft” ceramics that tend to have more temperature dependence, hysteresis and aging of properties.

Barium titanate (BaTiO_3) is of interest in the context of capacitors and piezoelectric transducers. It undergoes, on cooling, cubic-to-tetragonal, tetragonal-to-orthorhombic, and orthorhombic-to-rhombohedral transformations; above the Curie point, the crystal symmetry becomes insufficient for piezoelectricity. Pure BaTiO_3 has lower piezoelectric sensitivity ($d_{33} \approx 200\text{pC/N}$) than lead titanate zirconate. However, doped BaTiO_3 can exhibit competitive piezoelectricity in comparison with lead titanate zirconate ceramic with the benefit of being lead free and of having reduced hysteresis in comparison with “soft” compositions. Addition of dopants shifts the phase transformation temperatures; in particular,

the Curie point is shifted to lower temperature. Although this is a drawback for high temperature applications, the increased ambient temperature properties could be beneficial for applications of piezoelectric materials where service temperature is moderate. In particular, the rhombohedral crystal structure is considered to confer benefits in terms of piezoelectric sensitivity and strain capability.³ Pure barium titanate is rhombohedral only below -70°C but doped material can be rhombohedral at ambient temperature. Tunable phase transformation temperatures are also of interest in that physical properties such as dielectric permittivity, piezoelectricity, and viscoelastic damping can attain peaks in the vicinity of such transformation; moreover, they are pertinent in the context of novel composites that can achieve properties highly exceeding the bounds of classical composite theory.⁴ The electrical properties of $x\text{BaZrO}_3-(1-x)\text{BaTiO}_3$ solid solutions (the unit of x is “mol” but is often omitted for simplicity) have been studied by some researchers; however, most of the work focuses on either the hysteresis loops and strain properties of the system^{5,6} or the ferroelectric relaxor behaviors of this system with composition x usually higher than 0.2,⁷⁻¹² in which cases only one structural phase transformation remains between rhombohedral and cubic. Little work has been performed to systematically study the piezoelectric properties of $x\text{BaZrO}_3-(1-x)\text{BaTiO}_3$ system;^{13,14} therefore, the composition at which ambient temperature piezoelectric properties achieve maxima has not been accurately determined yet. Also, no work has been found hitherto to study the temperature dependence of piezoelectric properties of $x\text{BaZrO}_3-(1-x)\text{BaTiO}_3$ ceramics. The present study is intended to fill this gap. In this work, the temperature dependence of dielectric and piezoelectric properties of

^{a)}Author to whom correspondence should be addressed. Electronic mail: lakes@engr.wisc.edu.

$x\text{BaZrO}_3-(1-x)\text{BaTiO}_3$ system ($x < 0.2$) has been studied. The results show that $x\text{BaZrO}_3-(1-x)\text{BaTiO}_3$ solid solutions exhibit improved dielectric and piezoelectric properties as well as poling efficiency over pure BaTiO_3 . In particular, the best room temperature piezoelectric and electromechanical properties including d_{33} of 420 pC/N, d_{31} of -138 pC/N, and k_p of 49% have been achieved in $0.06\text{BaZrO}_3-0.94\text{BaTiO}_3$.

II. EXPERIMENTAL PROCEDURES

$x\text{BaZrO}_3-(1-x)\text{BaTiO}_3$ ceramics were synthesized by means of conventional solid state reaction method. BaTiO_3 (Alfa Aesar, 99.7% metal basis, $< 2 \mu\text{m}$ particle size) and BaZrO_3 (Alfa Aesar, 99% metal basis, $1\sim 2 \mu\text{m}$ particle size) powders were wet milled with DuPont™ Vertrel XF cleaning agent in a silicon nitride vial for 4 h with a high-energy planetary milling machine (SPEX SamplePrep 8000-series Mill/Mixer, SPEX CertiPrep PrepAid, Metuchen, NJ). The ball milled powder was calcinated at 1300°C for 15 h at atmospheric pressure. After remilling for 2 h, the powders were dried and pressed into disks of $\text{Ø}28.5 \times 5$ mm under a uniaxial pressure 110 MPa with a hydraulic press (Carver hydraulic laboratory pellet press, SPEX SamplePrep 3621 Carver® model C, Metuchen, NJ) of capacity of 24 000 lb at room temperature. Sintering was performed at 1400°C for 12 h at atmospheric pressure. Ramping up and down rates were $3\sim 4^\circ\text{C}/\text{min}$. To facilitate the composition homogeneity, five extra ball milling and sintering steps were performed with the same procedures as the first. Samples were kept inside an alumina crucible covered with an alumina lid and buried inside BaTiO_3 powder to avoid possible contamination from any residue left inside the furnace during sintering. The densities of these ceramics are about 93%–95% of the theoretical values. Optical microscopy observation showed an average grain size of $30 \mu\text{m}$ for the ceramics sintered for 12 h. For $0.06\text{BaZrO}_3-0.94\text{BaTiO}_3$, 100 h sintering (at atmospheric pressure) at 1400°C has also been performed, and an average grain size about $70 \mu\text{m}$ was observed.

Standard powder x-ray diffraction (Scintag PAD V XRD) has been performed to check phase purity and to determine lattice parameters for the doped BaTiO_3 . An x-ray diffraction spectrum of the pure BaTiO_3 has been incorporated for comparison.

Specimens of typical size $5 \times 3 \times 1 \text{ mm}^3$ were coated with conductive electrodes on two major surfaces by gold sputtering, and lead wires were fixed to the electrodes with silver paste. Electric-poling was performed in silicone oil at room temperature for 45 min under different dc electric fields. Dielectric measurements were performed at 10 kHz with a bridge circuit in which the specimen was connected in series with a known capacitor. Piezoelectric measurements were carried out by an optical method.¹⁵ Light from the optical fiber probe (MTI 2000 Fotonic Sensor, Latham, NY) was reflected from a mirror attached on the specimen surface to determine the specimen deformation in response to the applied ac electric fields ($5 \text{ V}_{\text{RMS}}/\text{mm}$ at 500 Hz). A lock-in amplifier (Stanford Research System SR 850 Sunnyvale, CA) served as both signal generator and receiver. In both dielectric and piezoelectric measurements, the temperature rate was about $0.03^\circ\text{C}/\text{s}$. It needs to be emphasized that we measured the reverse

piezoelectric coefficient in unit of pm/V. The equivalent unit pC/N is employed because it is more familiar. The dynamic piezoelectric coefficient was not measured via S-E (strain vs. dc electric field) loop method which also has the unit of pm/V. The electromechanical coupling coefficients were determined by a resonance and antiresonance method performed on the basis of IEEE standards^{16,17} with a circuit in which the specimen was connected in series with a known resistor.

III. RESULTS AND DISCUSSION

Figure 1 shows the optical micrographs of the $x\text{BaZrO}_3-(1-x)\text{BaTiO}_3$ ceramics. The ceramics sintered for 12 h have an average grain size about $30 \mu\text{m}$, while the ceramic ($0.06\text{BaZrO}_3-0.94\text{BaTiO}_3$) sintered for 100 h has an average grain size about $70 \mu\text{m}$. Much more complex and finer non- 180° domain structures were observed in doped ceramics compared with pure BaTiO_3 . In the orthorhombic phase, in addition to the 180° domain and 90° domain (with domain walls parallel to orthorhombic (110) planes), 60° domain (with domain walls parallel to orthorhombic (111) planes) has also been reported,¹⁸ whereas in the rhombohedral phase, 71° domain (domain walls are rhombohedral (100) planes) replaced 90° domain to accommodate the structure and internal stress.¹⁹

The room temperature XRD spectra of the sintered ceramics are shown in Figure 2. No secondary phase was observed indicating that BaZrO_3 has thoroughly diffused into the BaTiO_3 lattice. With increasing content of BaZrO_3 , the structure of BaTiO_3 changes from tetragonal to orthorhombic ($0 < x < 0.06$) and then to rhombohedral ($0.06 < x \leq 0.18$), and the diffraction peaks shift toward a lower angle as the substitution of Zr^{4+} ($\sim 0.72 \text{ \AA}$ ionic radius) for Ti^{4+} ($\sim 0.605 \text{ \AA}$ ionic radius) has expanded the BaTiO_3 lattice. The room temperature lattice parameters of $x\text{BaZrO}_3-(1-x)\text{BaTiO}_3$ have been calculated following the method proposed by Avrami and Tuller³ as follows: $x = 0$: tetragonal symmetry, $a = b = 3.992 \text{ \AA}$, $c = 4.031 \text{ \AA}$; $x = 0.04$: pseudo-monoclinic symmetry, $a = c = 4.001 \text{ \AA}$, $b = 4.021 \text{ \AA}$; $x = 0.06$: pseudo-monoclinic symmetry, $a = c = 4.017 \text{ \AA}$, $b = 4.023 \text{ \AA}$; $x = 0.08$: rhombohedral symmetry, $a = b = c = 4.020 \text{ \AA}$, $\alpha = \beta = \gamma = 89.95^\circ$; $x = 0.12$: rhombohedral symmetry, $a = b = c = 4.030 \text{ \AA}$, $\alpha = \beta = \gamma \geq 89.99^\circ$; $x = 0.18$: rhombohedral symmetry, $a = b = c = 4.042 \text{ \AA}$, $\alpha = \beta = \gamma \geq 89.99^\circ$.

The temperature dependence of the dielectric constant at 10 kHz for the sintered ceramics (1400°C 12 h) is shown in Figure 3. For pure BaTiO_3 , two sharp peaks are observed at about 20°C and 129°C in the temperature range accessed (-25°C to 180°C), corresponding to the phase transitions of tetragonal-orthorhombic (T_{O-T}) and cubic-tetragonal (T_c), respectively (the rhombohedral-orthorhombic transition occurs at about -75°C (Ref. 20)). With increasing content of BaZrO_3 , the Curie point shifts to lower temperature, whereas the other two transitions shift to higher temperatures. Three transformations merge into one transition when the concentration x reaches 0.12. The rhombohedral phase can be stabilized at room temperature when $x > 0.06$. At room temperature, the dielectric constant of the doped ceramics ($x = 0.04 - 0.18$) varies from 1731 to 6320, and the dielectric loss tangent ($\tan\delta$)

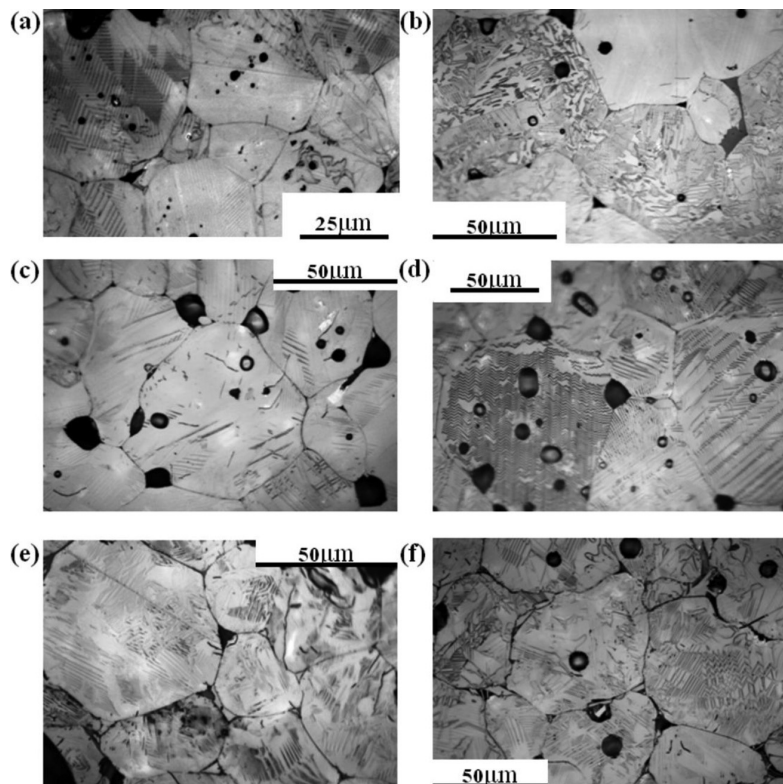


FIG. 1. Microstructures of the sintered $x\text{BaZrO}_3-(1-x)\text{BaTiO}_3$ ceramics (a) $x=0$, (b) $x=0.04$, (c) $x=0.06$ (12 h sintered), (d) $x=0.06$ (100 h sintered), (e) $x=0.08$, (f) $x=0.12$. Ceramics were not poled either before or during the microscopic observation.

varies from 1.1% to 7.2% (Table II), showing excellent dielectric properties. A phase diagram has been established based upon the dielectric measurements, as shown in Figure 4.

The steep increase in dielectric constant in the ferroelectric states over a wide range of temperature with increasing concentration x in the $x\text{BaZrO}_3-(1-x)\text{BaTiO}_3$ ceramics can be explained as follows. The internal stress caused by doping can be released by developing non- 180° domains with multiple configurations as the same mechanism in pure BaTiO_3 in which 90° domains are developed to relieve transformation stress when the ceramic is transformed from the paraelectric state into the ferroelectric state. Therefore, the total non- 180° domain area will increase and give rise to an improved dielectric response with increasing content of

BaZrO_3 because domain wall vibration is one contribution component to the dielectric constant²¹ (which is called orientational polarization). The other contribution component is lattice vibration, which is called ionic polarization.²² BaZrO_3 has an ideal cubic perovskite structure. Introduction of BaZrO_3 will distort the BaTiO_3 lattice and result in a structural transition at the microscale, but such a structural transition will be stabilized within localized regions rich of BaZrO_3 due to the constraint from adjacent structure. The interaction of dipoles is weak due to the phonon mode softening and structural relaxation in these regions, and the dipoles can be polarized to possess higher magnitudes under external alternative electric field, enhancing the dielectric responses; therefore, the accumulative dielectric responses of such localized constrained structural transition regions have also increased the overall dielectric constant of the doped ceramics.

For normal ferroelectrics, the dielectric constant above the Curie point follows the Curie-Weiss law: $\epsilon = C/(T - T_0)$, in which C is the Curie-Weiss constant, T_0 is the Curie-Weiss temperature. From a plot of inverse dielectric constant as a function of temperature (Fig. 3), the fitting results for the curve above the Curie point are summarized in Table I. The Curie-Weiss law fails to describe the dielectric constant behavior in the immediate vicinity of the Curie point. The deviation from the Curie-Weiss law is defined by ΔT_m (Ref. 23) with $\Delta T_m = T_{cw} - T_{\epsilon_m}$, where T_{cw} represents the temperature at which the dielectric constant starts to deviate from the Curie-Weiss law (in cooling), and T_{ϵ_m} corresponds to the temperature at which the dielectric constant reaches the maximum. The deviation of T_{cw} from T_{ϵ_m} is small in pure BaTiO_3

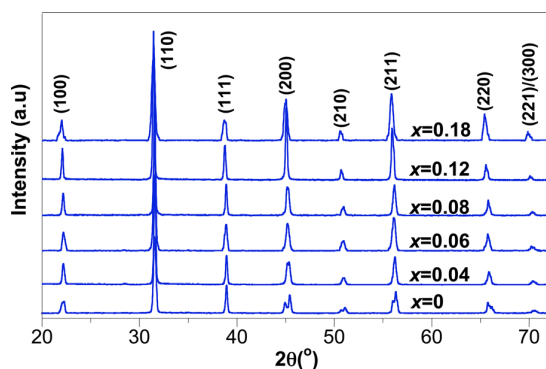


FIG. 2. Room temperature x-ray diffraction spectra of the sintered $x\text{BaZrO}_3-(1-x)\text{BaTiO}_3$ ceramics (12 h sintered) with $x=0, 0.04, 0.06, 0.08, 0.12$, and 0.18 .

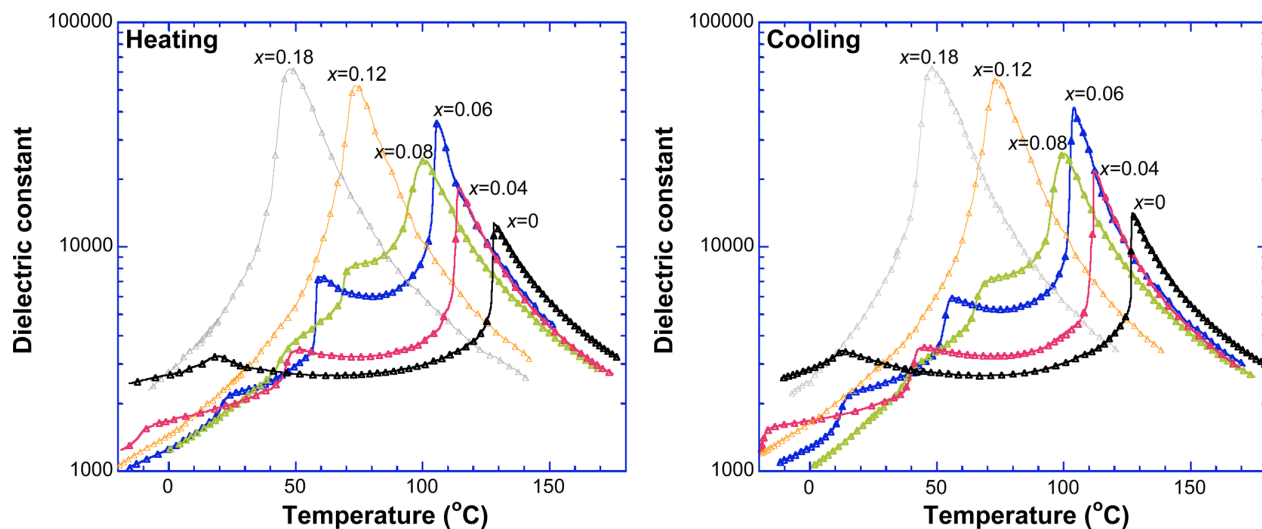


FIG. 3. Temperature dependence of dielectric constant at 10 kHz of the sintered $x\text{BaZrO}_3-(1-x)\text{BaTiO}_3$ ceramics (12 h sintered) with $x = 0, 0.04, 0.06, 0.08, 0.12,$ and 0.18 .

($\Delta T_m = 7^\circ\text{C}$) but becomes more and more prominent with increasing doping content ($\Delta T_m = 46^\circ\text{C}$ when $x = 0.18$). Such a phenomenon suggests that the diffuse transformation behavior has been enhanced with increasing content of BaZrO_3 . It can be seen from Figure 3 that the dielectric response (near T_c) continuously broadens with increasing BaZrO_3 content. The grade of broadening of phase transition is associated with the degree of freezing of paraelectric clusters to the ferroelectric phase.²⁴ The diffuseness of the ferroelectric phase transition can be expressed by the following empirical equation:²⁵ $1/\varepsilon - 1/\varepsilon_m = (T - T_{\varepsilon_m})^\gamma/C$, where γ and C are constant and γ ranges from 1 (ideal ferroelectric and equation reduces to Curie-Weiss law) to 2 (ideal relaxor). From a plot of $\log(1/$

$\varepsilon - 1/\varepsilon_m)$ against the $\log(T - T_{\varepsilon_m})$, the slope of the fitting curve is used to determine γ value (as shown in Figure 5). The γ value varies from 1.20 to 1.69 (see Table I, which summarizes the dielectric properties of the sintered ceramics).

Relaxor-like behavior, represented by an upper shift in transition temperature and a lowering of maximum permittivity with increasing frequency²³ and a strong frequency dependence of dielectric constant in the ferroelectric phase²⁶ has been found in many ferroelectric ceramics, such as $\text{PbMg}_{1/3}\text{Nb}_{2/3}\text{O}_3$ (PMN) and $\text{PbZn}_{1/3}\text{Nb}_{2/3}\text{O}_3$ (PZN),²⁷ and is generally attributed to the break of the ordered states by the introduction of dopant. The relaxor phase transition behavior has also been reported in $\text{Ba}(\text{Zr}_x\text{Ti}_{1-x})\text{O}_3$ system with x ranges from 0.3 to 0.75 and γ not less than 1.8.²⁶ In the solid solution of $x\text{BaZrO}_3-(1-x)\text{BaTiO}_3$, Zr^{4+} and Ti^{4+} occupy the B sites of the ABO_3 perovskite structure; the cation disorder will lead to the break of the ordered state at the microscopic level: in the superlattice, Zr^{4+} and Ti^{4+} are bonded to six O^{2-} , forming ZrO_6 (no displacement of Zr^{4+} with respect to octahedron center) and TiO_6 (Ti^{4+} displaces the octahedron center) octahedral clusters. The existence of the non-polar ZrO_6 clusters close to the TiO_6 clusters will cause local order-disorder into the BaTiO_3 matrix. On the other hand, since BaZrO_3 has an ideal cubic perovskite structure, the BaZrO_3 agglomerates could divide the BaTiO_3 macrodomains into microdomains, giving rise to the macroscopic composition fluctuation. Both micro- and macro-level disorders will contribute to the diffuse transition behavior of the $x\text{BaZrO}_3-(1-x)\text{BaTiO}_3$ ceramics ($0 < x \leq 0.18$). The frequency dependence of dielectric constant of $0.18\text{BaZrO}_3 - 0.82\text{BaTiO}_3$ as a function of temperature has been shown inset of Figure 5(a); however, the relaxor phase transition behavior was not clearly seen (in particular, the temperature shift of the dielectric constant maximum with frequency is barely detectable), and this is considered as the internal stress is not enough to reveal the relaxor behavior due to an insufficient mechanical impedance mismatch²⁶ between the ZrO_6

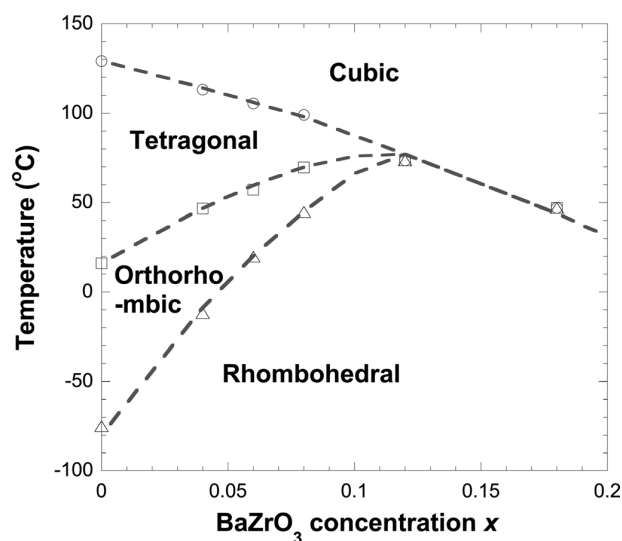


FIG. 4. Phase diagram of $x\text{BaZrO}_3-(1-x)\text{BaTiO}_3$ ceramics with $0 < x < 0.2$. Symbols are experimental data from dielectric studies, and dashed curves are guide to eyes. The rhombohedral-to-orthorhombic transition temperature for pure BaTiO_3 is obtained from Ref. 20.

TABLE I. The Curie-Weiss temperature (T_0), the Curie-Weiss constant (C), the temperature above which the dielectric constant follows the Curie-Weiss law (T_{cw}), the temperature corresponding to maximum dielectric constant value (T_{ϵ_m}), ΔT_m ($\Delta T_m = T_{cw} - T_{\epsilon_m}$), and the diffuseness coefficient (γ) for $x\text{BaZrO}_3$ - $(1-x)\text{BaTiO}_3$ ceramics at 10 kHz. Other than specified, the ceramics were sintered for 12 h at 1400 °C.

	$x=0$	$x=0.04$	$x=0.06$	$x=0.06$ (100 h)	$x=0.08$	$x=0.12$	$x=0.18$	$x=0$ (Ref. 21)
T_0 (°C)	115	109	108	112	103	85	67	108–113
C (°C)	194 000	179 000	188 000	187 000	192 000	187 000	189 000	123 000
T_{cw} (°C)	134	126	130	132	131	102	94	—
T_{ϵ_m} (°C)	127	112	104	107	100	74	48	120–122
ΔT_m (°C)	7	14	26	25	31	28	46	—
γ	1.07	1.20	1.27	1.25	1.32	1.58	1.69	—

and TiO_6 clusters. The diffuse phase transition behavior will finally evolve into relaxor-like phase transition behavior with higher concentration of ZrO_6 clusters. Actually, relaxor behavior was not observed in $x\text{BaZrO}_3$ - $(1-x)\text{BaTiO}_3$ when x is less than 0.25.²⁶

Figure 6 presents the piezoelectric properties (d_{33} and d_{31}) of the sintered ceramics $x\text{BaZrO}_3$ - $(1-x)\text{BaTiO}_3$ ($x=0, 0.04, 0.06, 0.08, 0.12,$ and 0.18) as a function of the electric poling field (electric poling was performed at room temperature for 45 min). The piezoelectric responses first increase rapidly with increasing poling field, but the rate slows down and the responses approach saturation with further increasing the poling field. Doped BaTiO_3 has comparable or higher d_{33} and $-d_{31}$ values than the pure material, and the piezoelectric coefficients reach maxima when the dopant concentration x is 0.06. The thresholds for the poling field to approach saturation in piezoelectric responses are much lower in doped ceramics, indicating that doping has improved the poling efficiency. It is known that the main effect of the poling field is to cause 180° domain reversals, whereas most of the non- 180° domains remain unaffected²⁸ under electric field. Doped ceramics should have a higher density of the non- 180° domains because forming non- 180° domains is the

most efficient way to relieve the internal stress caused by doping, and this explains why the doped ceramics can be much easily poled compared with pure BaTiO_3 . As 0.06 BaZrO_3 -0.94 BaTiO_3 brings the rhombohedral-orthorhombic transformation up to ambient temperature, the vanishing of the polarization anisotropy near the transition²⁹ and the enhanced mobility of domain walls make the ceramic to be extraordinarily “soft,” and it is possible to get fairly high piezoelectric responses ($d_{33} = 310$ pC/N; $d_{31} = -105$ pC/N) at a poling field as low as 100 V/mm at ambient temperature. The electrical properties of the 100 h sintered 0.06 BaZrO_3 -0.94 BaTiO_3 are superior to the 12 h sintered one, and this is attributed to their microstructure difference. The 100 h sintered ceramic presents a domain structure which consists of regular patterned uniform and fine (width about $1\mu\text{m}$) non- 180° domain bands (Figure 1(d)), whereas such a domain pattern was not observed in the 12 h sintered ceramic (Figure 1(c)), in which rather randomly patterned heterogeneous domain bands were observed. Such a domain pattern difference is attributed to, on the one hand, the extent of composition homogeneity, and, on the other hand, the grain size difference. Specifically, as stated before, BaZrO_3 will introduce internal stress which can be partially relieved

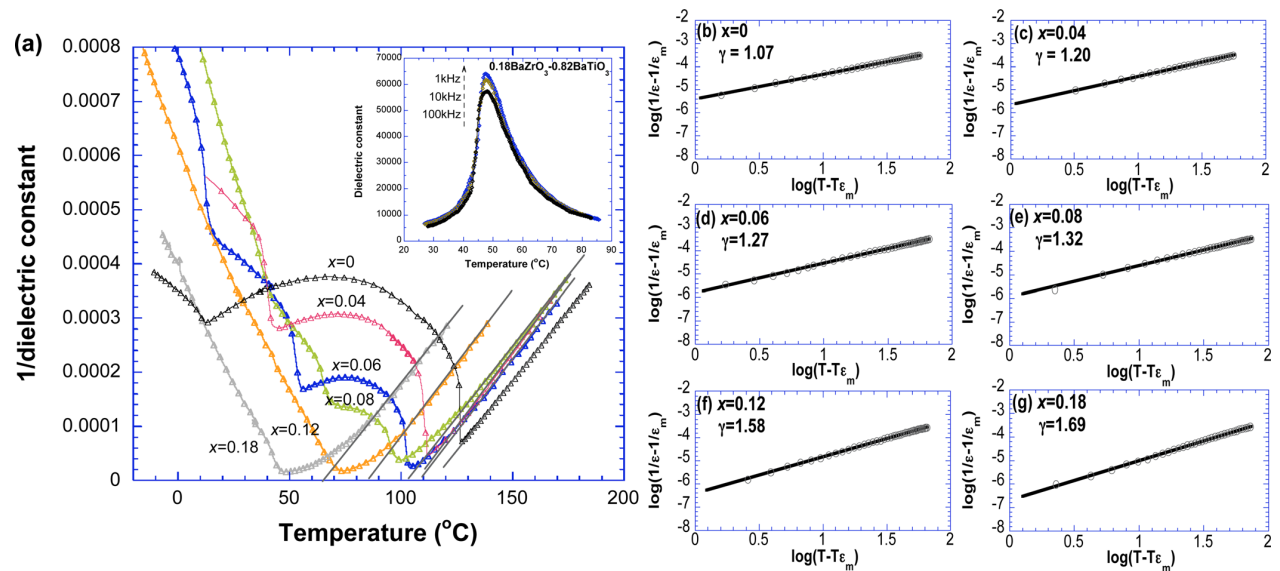


FIG. 5. (a) The inverse dielectric constant as a function of temperature at 10 kHz for $x\text{BaZrO}_3$ - $(1-x)\text{BaTiO}_3$ ceramics; (b)–(g) $\log(1/\epsilon - 1/\epsilon_m)$ vs. $\log(T - T_{\epsilon_m})$ at 10 kHz for $x\text{BaZrO}_3$ - $(1-x)\text{BaTiO}_3$ ceramics. Symbols are experimental data; the solid lines are fitting curves. Inset of (a) shows the frequency dependence of dielectric constant of 0.18 BaZrO_3 -0.82 BaTiO_3 vs. temperature.

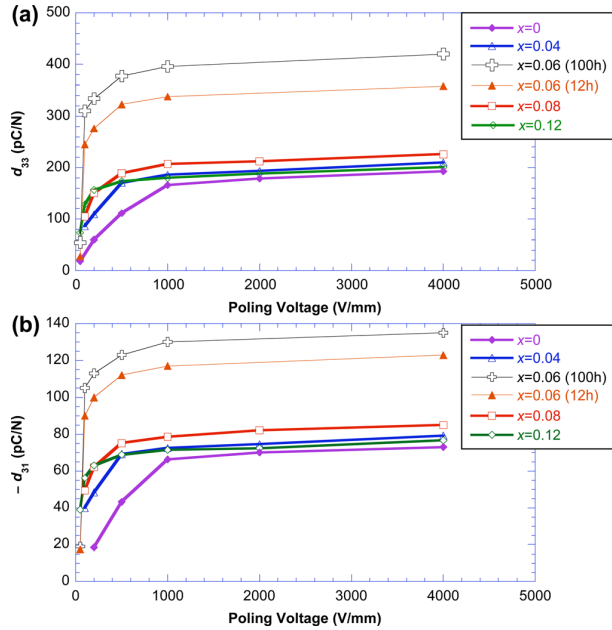


FIG. 6. Effect of poling field on d_{33} and $-d_{31}$ of the sintered $x\text{BaZrO}_3-(1-x)\text{BaTiO}_3$ ceramics.

by forming non- 180° domains. A longer sintering time can promote the diffusion of BaZrO_3 to achieve its homogeneous distribution inside the BaTiO_3 matrix, and hence the configuration of the formed non- 180° domains; as for the grain size contribution, it may have the following two aspects: First, a larger grain size will reduce the anisotropy of the grain orientations, and hence the overall anisotropy of domain orientations. Second, it is known²⁰ that the larger the grain size the smaller the internal stress near the grain boundaries and hence the internal stress inside the grain due to the elastic continuity. Since the domain structure will evolve from the grain boundary deep into the grain center accommodating to the internal stress configuration, the anisotropy of domain orientations (from grain boundary deep into grain center) within a particular grain will be reduced with increasing grain size.

The temperature dependence of d_{33} and d_{31} of the sintered ceramics is shown in Figure 7. Peaks were observed at the ferroelectric transformation temperatures, and these temperatures agree well with the dielectric measurements where peaks of the dielectric constant were observed. d_{33} and $-d_{31}$ increase dramatically from the rhombohedral phase towards the rhombohedral-to-orthorhombic transition but vary relatively slowly within the orthorhombic phase until the temperature approaches the vicinity of the orthorhombic-to-tetragonal transformation (this can be easily seen from Figure 7(d)). d_{33} and $-d_{31}$ then decrease rapidly within the tetragonal phase, and quickly smear out above T_c . Such a phenomenon indicates that the piezoelectric responses of the doped ceramics are more stable in the orthorhombic phase than in other ferroelectric phases. Such a behavior of d_{33} and $-d_{31}$ as a function of temperature is considered as the macroscopic representation of the evolution of spontaneous polarization with temperature. The lattice parameters of

BaTiO_3 as a function of temperature have been given by Kay and Vousden,¹⁸ lengths of “a” and “c” which determine the magnitude of spontaneous polarization (which is parallel to the plane formed by “a” and “c” axes of the monoclinic cell) are almost constant within the monoclinic phase (equivalent to the orthorhombic phase), whereas the lattice parameter “a” of the rhombohedral cell (in which the spontaneous polarization is along the body diagonal direction) is increasing and the lattice parameter “c” of the tetragonal cell (in which the spontaneous polarization is along “c” axis) is decreasing with increasing temperature within each phase, and so does the magnitude of the spontaneous polarization in the rhombohedral and tetragonal phases. Such conditions also apply to the doped BaTiO_3 . Peaks at transformation temperatures are mainly attributed to the lattice softening and structural relaxation (i.e., spontaneous strain) which lead to an increased domain mobility and unusual sensitivity to the external stresses or electric field (there is another mechanism named “constrained negative stiffness effect” which is considered to be able to contribute to the peaks near transformations and will be discussed later). When the dopant content x surpasses 0.08, only one transition remains, the rhombohedral phase will directly transform into the cubic phase near T_c giving rise to a single giant peak. The widths of the orthorhombic phase and the tetragonal phase gradually decrease with increasing dopant content, and the two phases finally merge into the transition peak corresponding to the rhombohedral-to-cubic transformation (with $x = 0.12$); therefore, it is reasonable to assume that such a single giant peak near T_c (corresponding to the rhombohedral-to-cubic transition) is attributed to a series of structural phase transitions at the microscopic scale where the coexistence of rhombohedral, orthorhombic, tetragonal, and cubic phases occurs. Actually, structural gradient exists microscopically in doped ceramics due to the presence of BaZrO_3 , and all the ferroelectric transformations of $x\text{BaZrO}_3-(1-x)\text{BaTiO}_3$ are hence the macroscopic representation of a series of microscopic structural phase transitions. Intensity of the transformation peaks depends on the volume fractions of different phases at the microscopic scale.

Figure 8 and Table II summarize the room temperature piezoelectric, dielectric, and electromechanical properties (d_{33} , d_{31} , ϵ , $\tan\delta$, k_p) of the sintered $x\text{BaZrO}_3-(1-x)\text{BaTiO}_3$ ceramics ($0 < x \leq 0.18$). The best properties occur at a composition of $x = 0.06$. Pure BaTiO_3 has d_{33} of 193 pC/N, d_{31} of -72 pC/N, and k_p of 29%. The 100 h sintered 0.06 $\text{BaZrO}_3-0.94\text{BaTiO}_3$ ceramic exhibits superior properties: $d_{33} = 420$ pC/N, $d_{31} = -138$ pC/N, and $k_p = 49\%$. The piezoelectric coefficients of 0.06 $\text{BaZrO}_3-0.94\text{BaTiO}_3$ are higher than unmodified PZT-8 ($d_{33} = 225$ pC/N, $d_{31} = -97$ pC/N) and PZT-4 ($d_{33} = 295$ pC/N, $d_{31} = -122$ pC/N), and even comparable to “soft” PZT-5 A ($d_{33} = 374$ pC/N, $d_{31} = -171$ pC/N).³⁰ The piezoelectric coefficients decrease rapidly when the composition is away from 0.06 $\text{BaZrO}_3-0.94\text{BaTiO}_3$ but are still comparable to the hard PZT-8.

The orthorhombic-tetragonal transition of pure BaTiO_3 is near room temperature; however, BaTiO_3 does not have as high ambient temperature piezoelectric properties as 0.06 $\text{BaZrO}_3-0.94\text{BaTiO}_3$ does, for which the rhombohedral-orthorhombic transition is also near room temperature. In

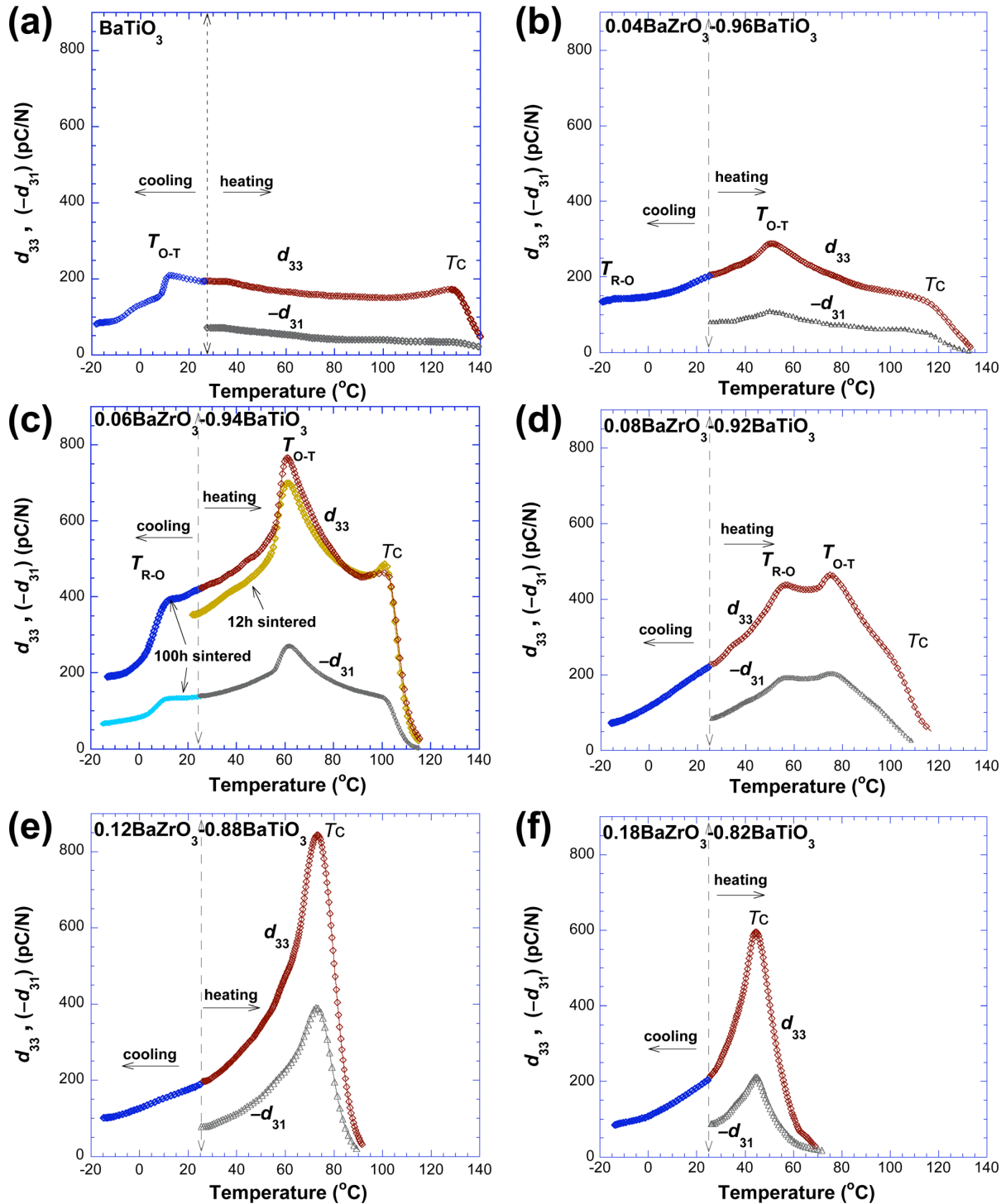


FIG. 7. Piezoelectric properties of the sintered $x\text{BaZrO}_3-(1-x)\text{BaTiO}_3$ ceramics as a function of temperature after poling at 4 kV/mm for 45 min at room temperature. (a) $x = 0$, (b) $x = 0.04$, (c) $x = 0.06$, (d) $x = 0.08$, (e) $x = 0.12$, and (f) $x = 0.18$.

addition, the doped ceramics with compositions away from $0.06\text{BaZrO}_3-0.94\text{BaTiO}_3$ still exhibited comparable or even higher room temperature piezoelectric coefficients compared with pure BaTiO_3 . Therefore, it is not only the macroscopic phase transformation from one ferroelectric state to another that contributes to the improved piezoelectric properties in

the doped ceramics but a series of microscopic phase transitions (i.e., coexistence of paraelectric state and more than one ferroelectric states due to the structural gradient at the microscopic scale caused by the presence of BaZrO_3 which has an ideal cubic perovskite structure) that mainly improves the overall piezoelectric responses. The difference is as

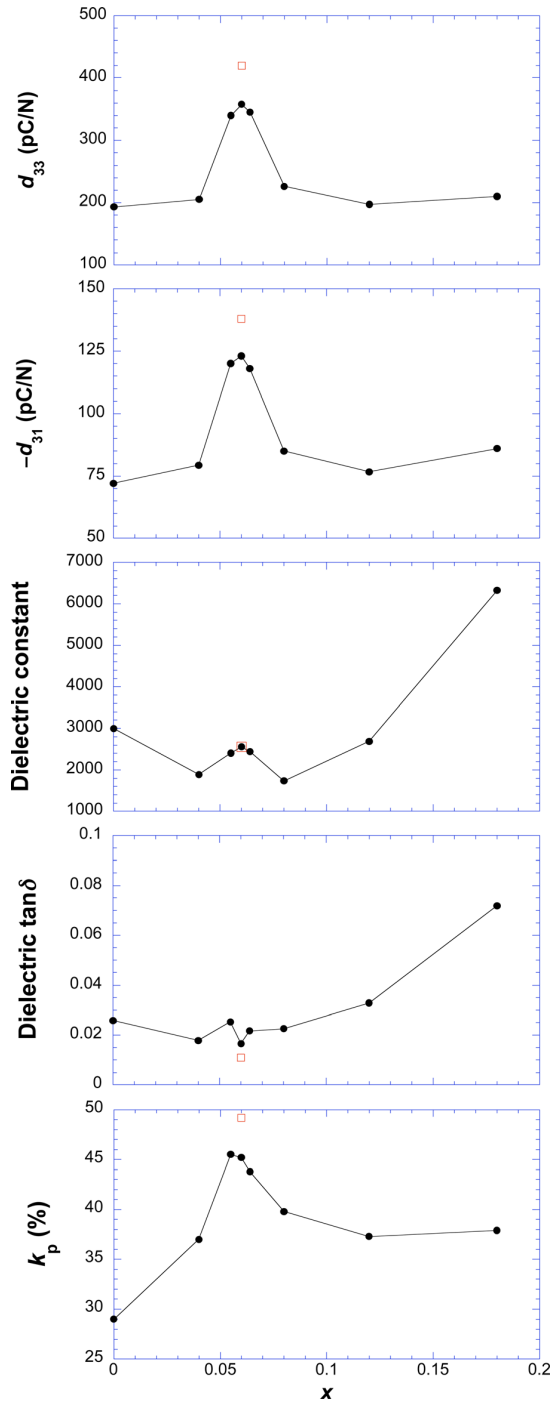


FIG. 8. Electrical properties of the sintered $x\text{BaZrO}_3-(1-x)\text{BaTiO}_3$ ceramics at room temperature. Properties of the 100 h sintered $0.06\text{BaZrO}_3-0.94\text{BaTiO}_3$ are represented by the hollow square. Poling was performed at 4 kV/mm for 45 min at room temperature.

follows: near room temperature, the phase transition occurs at the macroscopic scale (represented by the rhombohedral-orthorhombic transformation macroscopically, but structural transitions between other states are also available microscopically) in $0.06\text{BaZrO}_3-0.94\text{BaTiO}_3$; whereas it occurs locally inside the ceramics with compositions away from $0.06\text{BaZrO}_3-0.94\text{BaTiO}_3$. Another contribution to the improved piezoelectric

properties in doped ceramics is considered to be the effect of constrained negative stiffness. Negative stiffness describes a phenomenon that a reaction force in the same direction as imposed deformation⁴ and can occur in systems with store elastic energy, such as buckled tubes or ferroelastic/ferroelectric materials during phase transformations. Theoretical analysis has showed that constrained negative stiffness can induce extreme piezoelectric responses due to the coupling between electric field and strain field.³¹ Negative stiffness can be induced in BaTiO_3 based on ceramics by the following two mechanisms. The first mechanism applies at the macroscopic scale: negative stiffness is anticipated in the context of Landau theory of ferroelastic transformations. As the temperature T is lowered from a value above the transformation temperature, an energy function of strain (i.e., spontaneous strain) and temperature with a single minimum gradually flattens then develops two or more minima or potential wells. The curvature of this energy function represents an elastic modulus, so the flattening of the curve corresponds to a softening of the modulus near a critical temperature, and the reversed curvature at small strain represents a negative stiffness. Negative stiffness induced by phase transformations is unstable but can be stabilized in a polycrystalline material by mechanical boundary constraint provided by the grain or subgrain boundaries. The second mechanism occurs in localized regions: (1) near the grain or subgrain (subgrains are separated by BaZrO_3 agglomerates within each grain and are presented as the islands with different morphology inside the grain) boundaries, the schematic non- 180° domain structures are illustrated in Figure 9(a). The grain/subgrain boundary experiences compression and tensile stresses, and the non- 180° domains near this region can be modeled as a spring system consists of three springs (with spring constants of k_1 , k_2 , and k_3) jointed at a single point, forming a “Y” shape, as shown in Figure 9(b). k_1 and k_2 are relaxed and fixed in place by k_3 constraint which is provided by the grain or subgrain boundaries in the real material. During the phase transformations, the spontaneous polarizations switch (macroscopic phenomenon of TiO_6 octahedrons tilting), and the domain structures near the grain/subgrain boundaries are close to the configuration shown in Figure 9(c). The triple point can snap-through (refers to responses of buckled systems through instability regions) if k_3 constraint is not available, causing negative stiffness behavior. However, in the presence of the stress field near the grain/subgrain boundaries, such a snap-through will be restricted. Actually, such a constrained negative stiffness effect can play an important role in enhancing the piezoelectric responses far away from the transition temperatures at the subgrain boundaries in doped ceramics provided the subgrain is smaller than $10 \mu\text{m}$ in diameter, as the stressed volume can account for approximately 22% total volume of a grain in fine grain BaTiO_3 ,²¹ (2) at the microscopic scale (unit cell length scale), the schematic lattice structures near BaZrO_3 unit cells are illustrated in Figure 9[II]. BaZrO_3 is ideal perovskite cubic structure with no structural transformation below its melting point and has a stiffness about 2.4 times that of tetragonal BaTiO_3 .³² The BaTiO_3 unit cells in the immediate vicinity of BaZrO_3 will be shear deformed by an angle α/β with respect to BaTiO_3 unit cells far away from BaZrO_3 , giving

TABLE II. Density and electrical properties of the sintered $x\text{BaZrO}_3-(1-x)\text{BaTiO}_3$ ceramics. d_{33} , d_{31} , and k_p represent the responses after electric poling at 4 kV/mm for 45 min at room temperature.

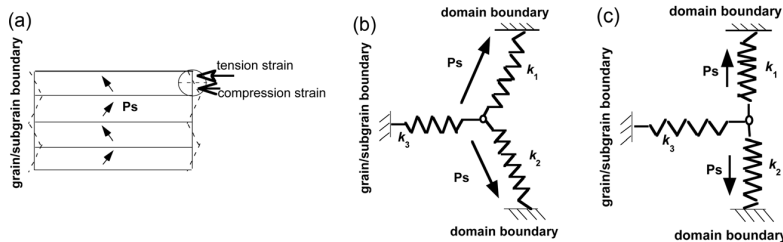
	$x=0$	$x=0.04$	$x=0.06$	$x=0.06$ (100 h)	$x=0.08$	$x=0.12$	$x=0.18$
ρ (% $\rho_{\text{theoretical}}$)	95.3	94.7	93.4	94.8	92.8	93.7	93.5
d_{33} (pC/N)	193	205	358	420	226	197	210
d_{31} (pC/N)	-72	-79	-123	-138	-85	-77	-86
ϵ (10 kHz)	2999	1890	2555	2562	1731	2690	6320
$\tan\delta$ (%)	2.6	1.8	1.7	1.1	2.3	3.3	7.2
k_p (%)	29	37	45	49	40	37	38

rise to stored elastic energy which will favor a snap-through effect if perturbation is available. Furthermore, the much more pre-strained domain configuration (i.e., 60° and 71° domain structures in the orthorhombic and rhombohedral, respectively^{18,19}) can allow more elastic energy to be stored and hence a more negative curvature on the free energy curve. Perturbation due to the lattice reconstruction during macroscopic phase transformations will alter the free energy at this region from the potential hill down to the valley, and a negative stiffness effect is entailed during this process. However, such a negative stiffness can be partially stabilized by the presence of BaZrO_3 which can be regarded as a stiff constraint. Both mechanisms discussed above are considered to contribute to the difference in piezoelectric responses between the pure and doped ceramics. Doped ceramics have much finer domain structures which could greatly enhance the density of negative stiffness elements. In pure BaTiO_3 , constraint comes from the grain and domain boundaries; whereas in doped ceramics, the BaZrO_3 centers provide additional mechanical constraint and hence more effectively stabilize the negative stiffness effect. Actually, evidence of strong constrained negative stiffness effect has been observed during viscoelastic measurements in the vicinity of phase transformations in $x\text{BaZrO}_3-(1-x)\text{BaTiO}_3$ system,³³ which suggests the assumed constrained negative stiffness effect could indeed play a role in enhancing the piezoelectric properties of doped ceramics.

IV. CONCLUSION

$x\text{BaZrO}_3-(1-x)\text{BaTiO}_3$ ceramics ($0 \leq x \leq 0.18$) synthesized via solid state reaction method exhibit piezoelectric coefficients comparable to those of commercial “hard” PZT-8 and PZT-4 and even to “soft” PZT-5 A. Doping lowered the Curie point and raised the transition temperatures of the other two lower temperature transformations, and the rhombohedral phase can be stabilized above the ambient temperature with $x > 0.06$. The diffuse phase transition behavior has been enhanced with increasing BaZrO_3 content and is attributed to both the macroscopic and microscopic disorders caused by the composition fluctuation; however, the relaxor behavior has not been observed when the composition $x \leq 0.18$. Doping of BaZrO_3 improves the poling efficiency of the ceramics, and extraordinarily “soft” character has been achieved in $0.06\text{BaZrO}_3-0.94\text{BaTiO}_3$, which brings the rhombohedral-orthorhombic transition up close to the ambient temperature. Peaks were observed in d_{33} and d_{31} in the vicinity of phase transformations. Greatly enhanced room temperature piezoelectric and electromechanical responses of $d_{33} = 420\text{pC/N}$, $d_{31} = -138\text{pC/N}$, and $k_p = 49\%$ are obtained at a composition $x = 0.06$. The piezoelectric properties of $0.06\text{BaZrO}_3-0.94\text{BaTiO}_3$ are competitive with “soft” PZT-5 A that has d_{33} of 374pC/N and d_{31} of -171pC/N . The improved piezoelectric responses in doped ceramics are mainly attributed to a series of microscopic phase transitions due to the presence of internal

[I] grain/subgrain boundary region



[II] BaZrO_3 rich zone

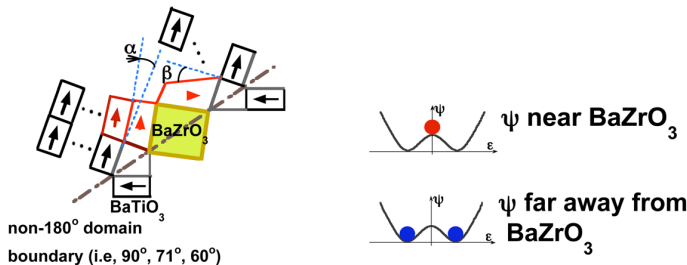


FIG. 9. [I] (a) Stress configurations near the grain/subgrain boundaries. (b) non- 180° domain model inside the grain or at the grain/subgrain boundary away from phase transformation, system is stable due to k_3 constraint. (c) Domain configuration near grain/subgrain boundary during phase transformation. Snap-through will be entailed if k_3 is not available. [II] Microstructure configuration near BaZrO_3 rich zone. The BaTiO_3 unit cells are shear deformed in the immediate vicinity of BaZrO_3 , but less stressed far away from BaZrO_3 rich zones. The arrow schematically represents the direction and magnitude of spontaneous polarization. Free energy profiles in the vicinity and far away from BaZrO_3 centers are shown at the side. The ball at the top of potential hill indicates a metastable condition of the lattice near the BaZrO_3 centers, while the balls at the bottom of the potential wells indicate a stable condition of the lattice far away from BaZrO_3 centers.

structural gradient; furthermore, the finer domain structures and the constrained negative stiffness effect are also considered as contributions to the superior piezoelectric properties in the doped ceramics.

ACKNOWLEDGMENTS

The authors gratefully acknowledge the support of DARPA and National Science Foundation.

- ¹D. A. Berlincourt, D. R. Curran, and H. Jaffe, in *Physical Acoustics*, edited by W. P. Mason (Academic Press, New York, 1964), Vol. 1A, p. 169.
- ²S. E. Park and T. R. Shrout, *J. Appl. Phys.* **82**, 1804 (1997).
- ³Y. Avrahami and H. L. Tuller, *J. Electroceram.* **13**, 463 (2004).
- ⁴R. Lakes, *Phys. Rev. Lett.* **86**, 2897 (2001).
- ⁵Z. Yu, C. Ang, R. Y. Guo, and A. S. Bhalla, *J. Appl. Phys.* **92**, 1489 (2002).
- ⁶Z. Yu, R. Y. Guo, and A. S. Bhalla, *Appl. Phys. Lett.* **77**, 1535 (2000).
- ⁷T. Maiti, R. Guo, and A. S. Bhalla, *J. Appl. Phys.* **100**, 114109 (2006).
- ⁸H. Maiwa, in *Advances in Ceramics-Electric and Magnetic Ceramics, Bioceramics, Ceramics and Environment*, edited by Costas Sikalidis (InTech, 2011), p. 1–20.
- ⁹S. Wada, H. Adachi, H. Kakemoto, H. Chazono, Y. Mizuno, H. Kishi, and T. Tsurumi, *J. Mater. Res.* **17**, 456 (2002).
- ¹⁰T. Tsurumi, Y. Yamamoto, H. Kakemoto, S. Wada, H. Chazono, and H. Kishi, *J. Mater. Res.* **17**, 755 (2002).
- ¹¹J. Ravez, C. Broustera, and A. Simon, *J. Mater. Chem.* **9**, 1609 (1999).
- ¹²C. Ciomaga, M. Viviani, M. T. Buscaglia, V. Buscaglia, L. Mitoseriu, A. Stancu, and P. Nanni, *Journal of the European Ceramic Society* **27**, 4061 (2007).
- ¹³W. Li, Z. J. Xu, R. Q. Chu, P. Fu, and G. Z. Zang, *Braz. J. Phys.* **40**, 353 (2010).
- ¹⁴N. Binhayeeniyi, P. Sukvisut, C. Thanachayanont, and S. Muensit, *Mater. Lett.* **64**, 305 (2010).
- ¹⁵J. T. Dawley, G. Teowee, B. J. J. Zelinski, and D. R. Uhlmann, "Piezoelectric Characterization of Bulk and Thin Film Ferroelectric Materials using Fiber Optics", *MRS Proceedings*, **433**, 317 (1996).
- ¹⁶IEEE Standard on Piezoelectricity (The Institute of Electrical and Electronics Engineers, Inc., New York, 1978).
- ¹⁷"Measurement of piezoelectric coupling in odd ceramic shapes," <http://www.morganelectroceramics.com/resources/technical-publications/> for Technical Publication TP-23.
- ¹⁸H. F. Kay and P. Vousden, *Philos. Mag.* **40**, 1019 (1949).
- ¹⁹P. W. Forsbergh, Jr., *Phys. Rev.* **76**, 1187 (1949).
- ²⁰K. Kinoshita and A. Yamaji, *J. Appl. Phys.* **47**, 371 (1976).
- ²¹G. Arlt, D. Hennings, and G. de With, *J. Appl. Phys.* **58**, 1619 (1985).
- ²²T. Hoshina, K. Takizawa, J. Y. Li, T. Kasama, H. Kakemoto, and T. Tsurumi, *Jpn. J. Appl. Phys., Part 1* **47**, 7607 (2008).
- ²³Y. P. Guo, K. Kakimoto, and H. Ohsato, *Solid State Commun.* **129**, 279 (2004).
- ²⁴G. Schmidt, *Ferroelectrics* **78**, 199 (1988).
- ²⁵K. Uchino and S. Nomura, *Ferroelectr. Lett. Sect.* **44**, 55 (1982).
- ²⁶T. Maiti, R. Guo, and A. S. Bhalla, *J. Am. Ceram. Soc.* **91**, 1769 (2008).
- ²⁷D. Damjanovic, P. Muralt, and N. Setter, *IEEE Sens. J.* **1**, 191 (2001).
- ²⁸B. Jaffe, W. R. Cook, Jr., and H. Jaffe, *Piezoelectric Ceramics* (Academic, London, 1971).
- ²⁹W. Liu and X. Ren, *Phys. Rev. Lett.* **103**, 257602 (2009).
- ³⁰Ferroperm Ltd., "*Piezoelectric Materials Data Book*", (Kvistgard, Denmark, 1996).
- ³¹Y. C. Wang and R. S. Lakes, *J. Appl. Phys.* **90**, 6458 (2001).
- ³²K. C. Goretta, E. T. Park, R. E. Koritala, M. M. Cuber, E. A. Pascual, N. Chen, A. R. de Arellano-López, and J. L. Routbort, *Physica C* **309**, 245 (1998).
- ³³L. Dong, D. Stone, and R. Lakes, *J. Mater. Res.* **26**, 1446 (2011).